RSC Advances

ROYAL SOCIETY OF CHEMISTRY

www.rsc.org/advances

Cite this: DOI: 10.1039/c0xx00000x

www.rsc.org/xxxxxx

ARTICLE TYPE

A new strategy to directly construct the hybrid luminescence-photothermal-magnetism multifunctional nanocomposites for cancer up-conversion imaging and photothermal therapy

Wenjia Liu, Guixia Liu*, Jinxian Wang, Xiangting Dong and Wensheng Yu

Received (in XXX, XXX) Xth XXXXXXXXX 20XX, Accepted Xth XXXXXXXXX 20XX
DOI: 10.1039/b000000x

Hybrid multifunctional nanocomposites with low toxicity have attracted considerable research attention in biomedical fields. Here, we report the development of the multifunctional Ag/$NaGdF_4$:Yb^{3+},Er^{3+} nanocomposites consisting of luminescence, photothermal and magnetism properties. The structure, morphology, composition and properties of the hybrid nanocomposites were confirmed by X-ray power diffraction (XRD), scanning electron microscope (SEM), energy-dispersive X-ray spectrometer (EDS), UV-Vis absorption (UV-Vis), fourier transform-infrared (FT-IR) spectra, up-conversion luminescence spectra, sensitive thermometer, vibrating sample magnetometer (VSM) and cytotoxicity assay, respectively. The results show that the $NaGdF_4$:Yb^{3+},Er^{3+} nanoparticles are coated on the surface of Ag nanospheres. The nanocomposites exhibit bright green up-conversion luminescence under irradiation with a 980 nm laser and magnetism property with room-temperature magnetization value of 1.5669 emu g^{-1} at 20 kOe. In addition, we examined the temperature changes when the solutions of samples were exposed to a 980 nm NIR laser. *In vitro* cell cytotoxicity assays on U87MG cancer cells demonstrate that the nanocomposites exhibit low toxicity and good biocompatibility. Furthermore, the up-conversion luminescence imaging and the photothermal therapy of Ag/$NaGdF_4$:Yb^{3+},Er^{3+} nanocomposites were realized under 980 nm NIR laser excitation, confirming that the nanocomposites are potential candidates as bioimaging and photothermal agents. Taken together, these results indicate that the prepared hybrid Ag/$NaGdF_4$:Yb^{3+},Er^{3+} multifunctional nanocomposites based luminescence-photothermal-magnetism properties have great promise in the future bioimaging and targeted therapy of tumor.

1. Introduction

Currently, design and synthesis of hybrid multifunctional nanocomposites combining two or more different properties into one single entity have attracted tremendous interest in biomedical fields due to their potential applications, such as targeting, bioimaging, diagnosis, drug delivery, tumor therapy and so on.[1-15] Among them, lanthanide doped up-conversion nanocrystals, which can convert a longer wavelength excitation to shorter wavelength emission *via* a two- or multi-photon process,[16,17] have emerged as alternative ideal up-conversion imaging agents because of their high quantum yields, sharp emission lines, low photobleaching and blinking, low toxicity, low photodamage to living organisms, good penetration depth and an improved ratio of signal to noise compared to conventional organic dyes and semiconductor quantum dots.[18-23] Meanwhile, the $AREF_4$ (A = alkali metal, RE = rare earth) fluorides nanomaterials have been reported as the outstanding up-conversion luminescence host materials, in comparison with AYF_4 or $ALuF_4$ nanocrystals, lanthanide doped $NaGdF_4$ nanocrystals can not only achieve ideally up-conversion luminescence, but also exhibit paramagnetism due to the intrinsic magnetic moment of Gd^{3+} ions. The Yb^{3+} ions, which were regularly used as sensitizers for the up-conversion process, have a large absorption cross-section at 980 nm.[24,25] In addition, the Yb^{3+} ions have a simple energy level scheme, in which the $^2F_{7/2}$-$^2F_{5/2}$ transition is resonant with f-f transitions of a few lanthanide ions, including Er^{3+}, Ho^{3+} and Tm^{3+} ions, that is why these elements constitute the most efficient up-converting activators.[26-28] And we all have known that the ultraviolet and visible lights had weak penetration by only a few millimeters, but near-infrared (NIR) have deep one in tissues by one to several centimeters.[29-35] Excitation with NIR increases their possible application viability because the biological tissues are in the NIR range, where the blood and tissues have the minimal adsorption, thus achieving deep penetration depth of light in the so-called therapeutic window.[36-40] Hence, the Yb^{3+}-Er^{3+} ions co-doped $NaGdF_4$ nanocrystal, a preferable up-conversion luminescent nanomaterial, as dual-mode imaging agents, could simultaneously yield up-conversion emission and magnetism properties for tumor cells imaging.

The NIR not only have deep tissues penetration, but also have the fascinating heating effect; in this case, the NIR are widely used for photothermal therapy in biomedical fields. In order to absorb more NIR, the noble metal nanoparticles are always acted

as the NIR absorption agents,[41-46] which have the photothermal transduction property, they can convert the NIR to heat owing to the surface plasmon resonance or energy transfer band. In plasmonics, metal nanostructures can work as antennae to convert light into localized electric fields surrounding the noble metal nanoparticles.[47,48] The photothermal effect is a strong nonradiative process caused by the surface of electrons that have a strong oscillation when the noble metal nanomaterials are irradiated with NIR.[49] Noble metal nanomaterials stand for a class of important and intensively researched nanomaterials because of their high surface to volume ratio and high surface free energy of nanoparticles with small size,[50,51] as well as, the optical properties of absorbing the lights in a broad range from the visible to the NIR region are always represented absorption agents to improve the effect of photothermal therapy at the NIR region. Here, we use Ag nanoparticles to act as the NIR absorption agents, due to the fact that they have lower price, higher stability and easier preparation method than other kinds of noble metal. The programmer localizes the NIR absorption agent of Ag nanoparticles at the tumor site and irradiates the site with the NIR to "bake" the tumor cells,[52-54] in this way; we can kill the tumor cells.

In the present work, we prepared the hybrid Ag/$NaGdF_4$:Yb^{3+},Er^{3+} multifunctional nanocomposites consisting of luminescence, photothermal and magnetism properties. The advantages of the hybrid multifunctional nanocomposites are particularized here. First, the Yb^{3+}-Er^{3+} ions co-doped $NaGdF_4$ nanoparticles can simultaneously achieve up-conversion luminescence and magnetism properties at room temperature. Second, the incorporation of Ag nanoparticles can provide intriguing photothermal conduction property; they can convert the NIR to heat by the surface plasmon resonance (SPR) property. More importantly, the Ag nanoparticles and lanthanide doped fluoride nanocrystals have good biocompatibility. The PVP was introduced into the reaction system, which always used as a significant dispersant and surfactant agent to disperse the nanoparticles and govern the nanoparticles size. The up-conversion luminescence and photothermal effect of the Ag/$NaGdF_4$:Yb^{3+},Er^{3+} nanocomposites are examined under excitation from a 980 nm laser at room temperature. In addition, the magnetism property of nanocomposites has been examined at room temperature. In order to apply in the biomedical fields, the biocompatibility of the Ag/$NaGdF_4$:Yb^{3+},Er^{3+} multifunctional nanocomposites is also evaluated by the MTT assay and expressed as a percentage of the control on U87MG cells. At last, the up-conversion luminescence imaging and the photothermal therapy of the hybrid Ag/$NaGdF_4$:Yb^{3+},Er^{3+} nanocomposites were realized under 980 nm NIR laser excitation, confirming that the nanocomposites potential are candidates as bioimaging and photothermal agents. Therefore, the hybrid Ag/$NaGdF_4$:Yb^{3+},Er^{3+} luminescence-photothermal-magnetism nanocomposites can realize cells imaging and tumor photothermal therapy in the biomedical fields.

2. Experimental sections

Chemicals

As starting materials, all of the chemical reagents used in this investigation were of analytical grade and were received without further purification. Gadolinium oxide (Gd_2O_3), ytterbium oxide (Yb_2O_3), erbium oxide (Er_2O_3), sodium fluoride (NaF), polyvinylpyrrolidone (PVP, K=30), nitric acid (HNO_3), ethylenediamine ($C_2H_8N_2$), ethylene glycol (EG), acetone and ethanol were purchased from Sinopharm Chemical Reagent Co., Ltd. And silver nitrate ($AgNO_3$) was purchased from Aladdin. Ethylene glycol (EG) and deionized water (DI water) were used as the common solvent in this study. Aqueous solutions of $RE(NO_3)_3$ (RE=Gd, Yb, Er) were obtained by dissolving the rare earth oxides RE_2O_3 in dilute HNO_3 solution (15 mol L^{-1}) under heating with agitation in ambient atmosphere by evaporating the water and adding a certain amount of ethylene glycol (EG).

Synthesis of amino-functional Ag nanoparticles

The amino-functional Ag nanoparticles were prepared by the solvent-thermal method. Briefly, $AgNO_3$ (0.1 g) and PVP (1.0 g, K=30) were dissolved in EG (35 mL) with continuous stirring at room temperature to form a homogeneous solution, followed by the addition of $C_2H_8N_2$ (3 mL). The mixture was stirred vigorously for 30 min and then transferred to a Teflon bottle held in a stainless steel autoclave (50 mL capacity). The autoclave was heated at 130 °C for 1 h. Finally, as the autoclave was naturally cooled to room temperature, the silver was separated by centrifugation at 9000 rpm for 8 min with a large amount of acetone. The Ag nanoparticles were washed with DI water and ethanol at least three times, and then dried in air at 60 °C for 24 h.

Synthesis of Ag/$NaGdF_4$:Yb^{3+},Er^{3+} nanocomposites

The as-prepared 10 mg of amino-functional Ag nanoparticles were added into DI water by sonicating to form a clear solution in a three-necked flask. A total of 0.5 mmol of $Gd(NO_3)_3$, $Yb(NO_3)_3$ and $Er(NO_3)_3$ (molar ratio Gd: Yb: Er = 78: 20: 2) were added into above solution at room temperature. After stirring for 30 min, PVP (0.45 g, K=30), NaF (6 mmol) and EG (10 mL) were added into the above solution. Under Ar gas flow, the solution was vigorously stirred until to form a homogeneous solution and the reaction temperature was raised to 180 °C. The solution was refluxed for 4 h before cooling down to room temperature under Ar gas flow. The products were separated by centrifugation at 8000 rpm for 5 min, thoroughly washed with DI water and ethanol in sequence each several times, and further dried at 60 °C overnight. The schematic illustration of the nanocomposites was presented in Fig. 1.

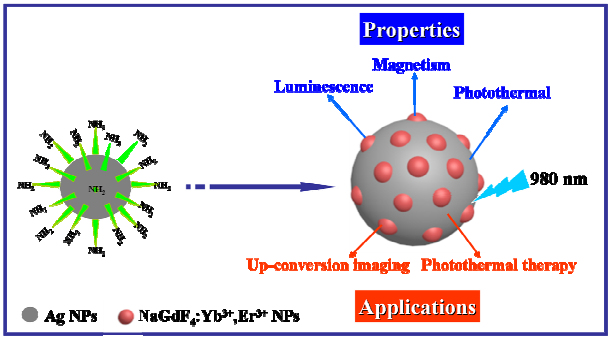

Fig. 1 Schematic illustration of the preparation of multifunctional Ag/$NaGdF_4$:Yb^{3+},Er^{3+} nanocomposites for up-conversion luminescence imaging and photothermal therapy.

The $C_2H_8N_2$ was added in the process of preparing Ag nanoparticles, which can modify the surface of the Ag nanoparticles by -NH_2 group, in this way, we can achieve the purpose of using -NH_2 group to link Ag and rare earth ions. Thus, the $NaGdF_4$:Yb^{3+},Er^{3+} nanopartilces coated on the surface of Ag nanopartilces.

Cytotoxicity assay

The cytotoxicity was measured through the colorimetric assay by using the 3-(4, 5-dimethylthiazol-2-yl)-2, 5-diphenyltetrazolium bromide (MTT) assays on U87MG cells. The U87MG cells were plated at a density of 5×10^4 cells per well in 96-well plates under a humidified 5% CO_2 at 37 °C for 24 h. The cells were treated with different concentration of 0.05, 0.10, 0.20, 0.25, 0.50 and 1.00 mg mL^{-1} of the Ag/$NaGdF_4$:Yb^{3+},Er^{3+} nanocomposites and incubated for another 24 h at 37 °C under 5% CO_2. The cells were cultured without nanocomposites materials which were chosen as controls, and each concentration was examined in 3 wells. After that, the cells were washed several times with phosphate buffered saline (PBS) and treated with MTT solution at 37 °C for 4 h in an incubator with 5% CO_2. MTT was removed and 150 μL of dimethyl sulphoxide (DMSO) was added into each well. Finally, the optical density was measured at 490 nm using an absorbance microplate reader Tquant (BioTEK, USA). The cell viability was calculated by the following equation: cell viability (%) = (absorbance of treat wells – absorbance of medium control wells)/(absorbance of untreated wells – absorbance of medium control wells) × 100%.

Up-conversion luminescence imaging of nanocomposites

The up-conversion luminescence imaging of U87MG cells was illuminated with an inverted florescence microscope (Nikon Ti-S), and an external CW 980 nm laser diode. The U87MG cells (1×10^4 per well) were first seeded in 6-well culture plates and cultured for 24 h at 37 °C under 5% CO_2, and were incubated with the hybrid Ag/$NaGdF_4$:Yb^{3+},Er^{3+} nanocomposites at 37 °C for different times (30 min, 2h and 4 h). After that, the cells were washed several times with phosphate buffered saline (PBS). The bright field, cell nucleus and up-conversion luminescence imaging of U87MG cells were obtained.

Photothermal therapy of nanocomposites

In vitro photothermal therapy of the hybrid Ag/$NaGdF_4$:Yb^{3+},Er^{3+} nanocomposites was assayed against U87MG cancer cells. The cells were first plated out in 96-well plates at a density of 1×10^4 per well and were cultured overnight to allow cell attachment. And then, the cells were treated by a cultured medium with 0.25 mg mL^{-1} of nanocomposites. After 20 h of incubation time, the free nanocomposites were separated from cultured medium by rinsing several times with PBS. The cells were then irradiated with a 1.2 W cm^{-2} laser diode at a wavelength of 980 nm for 0, 1, 2, 4 and 8 min. The cell viability was calculated by MTT assay, which were always used to examine the photothermal therapy of Ag/$NaGdF_4$:Yb^{3+},Er^{3+} nanocomposites.

Characterizations

The purity and phase structure of the products were examined by X-ray powder diffraction (XRD) using a Bruker D8 FOCUS with Cu Kα radiation (λ=1.54056 Å) and Ni filter; scanning speed, step length and diffraction range were 10° min^{-1}, 0.1° and 10-70°, respectively. The morphology and composition of the products were observed by a field emission scanning electron microscope (FESEM) equipped with an energy-dispersive X-ray spectrometer (EDS). The UV-Vis absorption spectra were obtained by a Shimadzu UV-2450 spectrophotometer. Fourier Transform infrared (FT-IR) spectra were examined on a BRUKER Vertex 70 IR spectrophotometer using KBr pellet technique. The up-conversion emission spectra were acquired by a HITACHI F-7000 fluorescence spectrophotometer coupled with a 980 nm laser source. The magnetism performance of the nanocomposites was measured using a commercial Quantum Design superconducting quantum interference device magnetometer (MPMS SQUID XL, San Diego, California, America). The magnetization as a function of the applied magnetic field ranging from -20 to 20 kOe was examined by a vibrating sample magnetometer (VSM) at room temperature. The solutions of products were placed in quartz cuvettes and irradiated with a 980 nm near-infrared (NIR) laser (1.2 W cm^{-2}) for 10 min. And the temperature of the solutions was acquired by a HTC3500C sensitive thermometer. The up-conversion luminescence microscopy (UCLM) instrument was rebuilt on an inverted florescence microscope (Nikon Ti-S), and an external CW 980 nm laser diode was illuminated onto the products.

3. Results and discussion

Structural, morphology and composition

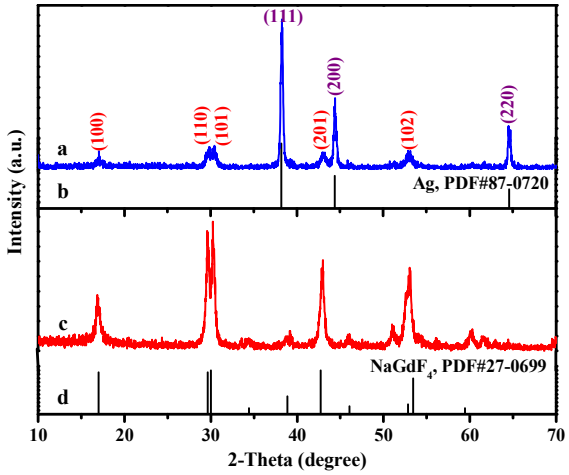

Fig. 2 The XRD patterns of Ag/$NaGdF_4$:Yb^{3+},Er^{3+} nanocomposites (a), $NaGdF_4$:Yb^{3+},Er^{3+} nanoparticles (c), and the standard cards for Ag (b) and β-$NaGdF_4$ (d) as references.

The XRD patterns of the as-prepared $NaGdF_4$:Yb^{3+},Er^{3+} nanoparticles and Ag/$NaGdF_4$:Yb^{3+},Er^{3+} nanocomposites are shown in Fig. 2, which have been recorded from 10° to 70° range. From Fig. 2c, it is noted that all the diffraction peaks of the as-prepared $NaGdF_4$:Yb^{3+},Er^{3+} nanoparticles can be assigned to the pure hexagonal phase of $NaGdF_4$, and they match well with the standard values of JCPDS card (PDF#27-0699) (Fig. 2d). No other diffraction peaks or impurities are detected, implying that the co-doped Yb^{3+}, Er^{3+} ions have no impact on the host crystal phase structure. However, compared with the standard data, the examined XRD peaks have a slight shift to larger angles, owing

to the doped ions occupy sites in the host depending on the effective radii of the nine-coordinated Yb^{3+} (radius 1.182 Å), and the nine-coordinated Er^{3+} (radius 1.202 Å) ions are smaller than those of the nine-coordinated Gd^{3+} (radius 1.247 Å) ions. As shown in Fig. 2a, it can be found that besides the diffraction peaks of β-$NaGdF_4$:Yb^{3+},Er^{3+}, several additional diffraction peaks at 38.2°, 44.4° and 64.6° are corresponded to the (111), (200) and (220) lattice planes of silver (PDF#87-0720) (Fig. 2b). The XRD pattern indicates the existence of both silver and $NaGdF_4$:Yb^{3+},Er^{3+} in the formed Ag/$NaGdF_4$:Yb^{3+},Er^{3+} hybrid nanocomposites.

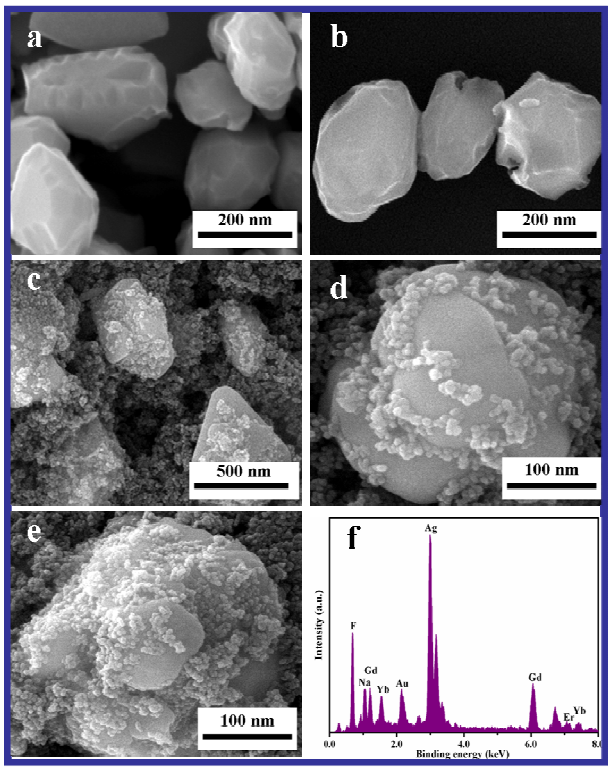

Fig. 3 The SEM images of Ag nanoparticles (a, b), Ag/$NaGdF_4$:Yb^{3+},Er^{3+} nanocomposites (c, d, e) and the EDS spectrum of Ag/$NaGdF_4$:Yb^{3+},Er^{3+} nanocomposites (f).

The morphology and size details of Ag nanoparticles and Ag/$NaGdF_4$:Yb^{3+},Er^{3+} nanocomposites were characterized by SEM, the images were exhibited in Fig. 3. It is noted that the as-prepared Ag nanoparticles are approximate irregular ellipsoidal shape with rough surface, and the mean diameter of the particles is about 200 nm (Fig. 3a and 3b). As shown in Fig. 3c, the SEM image of nanocomposites shows that the $NaGdF_4$:Yb^{3+},Er^{3+} nanoparticles are coated on the surface of Ag nanoparticles, and the $NaGdF_4$:Yb^{3+},Er^{3+} nanoparticles are not uniform with some aggregate. From the higher magnification SEM images of a single Ag/$NaGdF_4$:Yb^{3+},Er^{3+} nanoparticle presented in Fig. 3d and 3e, we clearly observe that the Ag nanoparticle is surrounded by the $NaGdF_4$:Yb^{3+},Er^{3+} nanoparticles. The average diameter of $NaGdF_4$:Yb^{3+},Er^{3+} nanoparticles is about 10 nm, the diameter of the nanocomposites is slightly larger than individual Ag nanoparticles. And the Ag/$NaGdF_4$:Yb^{3+},Er^{3+} nanocomposites have a relative rough surface, which can be easily modified to improve the photothermal transduction efficiency. To analyze the elemental composition, the EDS spectrum of hybrid Ag/$NaGdF_4$:Yb^{3+},Er^{3+} nanocomposites is displayed in Fig. 3f, it is noted that the sample contains Na, Gd, F, Yb, Er, Ag and Au elements. Among those elements, Na, Gd, F, Yb, Er and Ag elements in the EDS spectrum confirm the formation of the Ag/$NaGdF_4$:Yb^{3+},Er^{3+}. In addition to those elements, there is a single peak of Au coming from spraying gold process. Combined with the above SEM images and XRD patterns, it is once again proved that the hybrid Ag/$NaGdF_4$:Yb^{3+},Er^{3+} multifunctional nanocomposites are prepared.

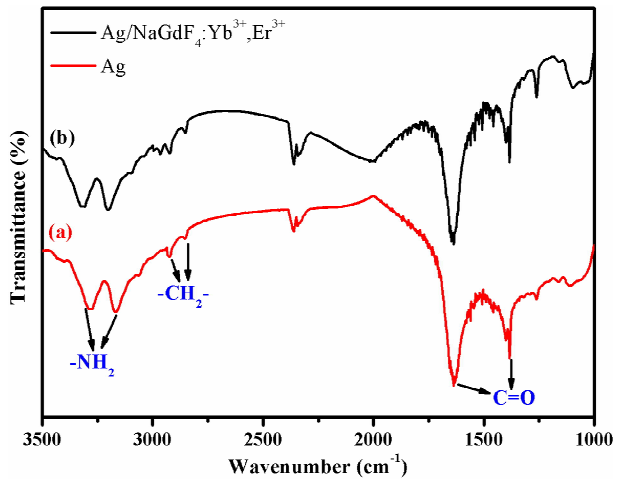

Fig. 4 FT-IR spectra of Ag nanoparticles (a) and Ag/$NaGdF_4$:Yb^{3+},Er^{3+} nanocomposites (b).

The FT-IR spectra of Ag nanoparticles (a) and Ag/$NaGdF_4$:Yb^{3+},Er^{3+} nanocomposites (b) are given in Fig. 4. The spectra show two tip peaks in the range of 3200 to 3400 cm^{-1}, which may be attributed to the stretching vibration of -NH_2 groups of $C_2H_8N_2$ molecules.[55] It implied that the -NH_2 groups are coated on the surface of Ag nanoparticles. At the same time, the absorption peaks at 2925, 2853 cm^{-1} can be assigned to the asymmetric and symmetric stretching vibration of C-H in the -CH_2 group in the $C_2H_8N_2$ and PVP, the bands at 1637, 1385 cm^{-1} are due to the stretching vibration of C=O groups from PVP, and the band at 1095 cm^{-1} is ascribed to the bending vibration of C=O groups from PVP. This phenomenon may be merely due to the addition of PVP in the preparation of the products. This result confirms that the $C_2H_8N_2$ and PVP molecules consist in the hybrid multifunctional Ag/$NaGdF_4$:Yb^{3+},Er^{3+} nanocomposites.

Optical properties

The UV-Vis absorption spectra experiments were performed to confirm the surface plasmon resonance (SPR) absorption of silver nanoparticles. As depicted in Fig. 5, the UV-Vis absorption peaks observed at 441 and 451 nm are assigned to the SPR absorption of Ag nanoparticles. Comparing the two absorption peaks of Ag nanoparticles and Ag/$NaGdF_4$:Yb^{3+},Er^{3+} nanocomposites at room temperature, it can be found that the peak of nanocomposites has a smaller blue shift about 10 nm to the pure Ag nanoparticles, which confirmed that the $NaGdF_4$:Yb^{3+},Er^{3+} nanoparticles have little effect on the SPR absorption property of Ag nanoparticles.

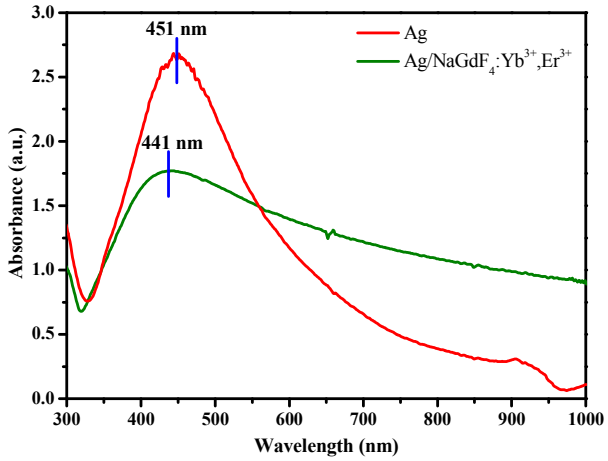

Fig. 5 UV-Vis spectra of Ag nanoparticles and Ag/$NaGdF_4$:Yb^{3+},Er^{3+} nanocomposites in water.

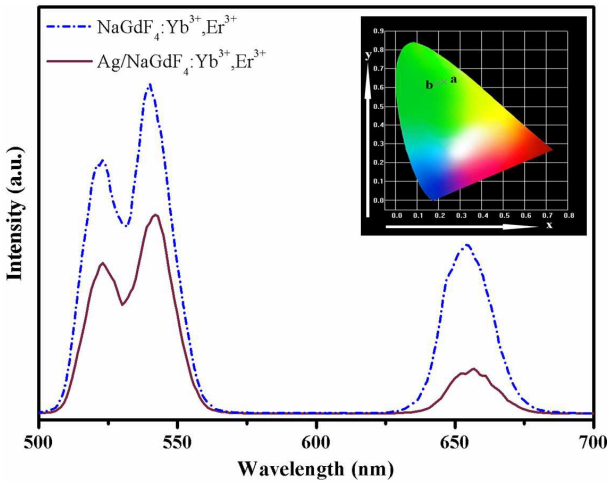

Fig. 6 Up-conversion luminescence spectra of the $NaGdF_4$:Yb^{3+},Er^{3+} nanoparticles and Ag/$NaGdF_4$:Yb^{3+},Er^{3+} nanocomposites under 980 laser excitation. Inset shows the CIE 1931 chromaticity diagram of $NaGdF_4$:Yb^{3+},Er^{3+} nanoparticles (a) and Ag/$NaGdF_4$:Yb^{3+},Er^{3+} nanocomposites (b).

It is well known that the Yb^{3+}-Er^{3+} ions co-doped rare earth fluorides emit strong green emission under conventional 980 nm laser excitation. Fig. 6 displays the up-conversion luminescence spectra and the CIE 1931 chromaticity diagram of $NaGdF_4$:Yb^{3+},Er^{3+} nanoparticles and Ag/$NaGdF_4$:Yb^{3+},Er^{3+} nanocomposites at room temperature under 980 nm laser excitation. From the up-conversion emission spectra, three main characteristic emission peaks at 523, 540 nm of green emission and 655 nm of red emission are assigned to the $^2H_{11/2}\rightarrow{}^4I_{15/2}$, $^4S_{3/2}\rightarrow{}^4I_{15/2}$ and $^4F_{9/2}\rightarrow{}^4I_{15/2}$ transitions of Er^{3+} ions, respectively. Under excitation at 980 nm, the Yb^{3+} ions could be excited from ground state $^2F_{7/2}$ to the excited state $^2F_{5/2}$ and returned to the ground state again, the released energy could be non-radiatively transferred to Er^{3+} ions, and excited Er^{3+} ions to the corresponding excited level. In addition, the positions of the up-conversion emission peaks in nanocomposites are in accordance with those of the pure $NaGdF_4$:Yb^{3+},Er^{3+} nanoparticles, confirming that the up-conversion processes from Yb^{3+} to Er^{3+} ions have not changed through introduction of Ag nanoparticles. But after introducing Ag nanoparticles, the emission intensity of the hybrid Ag/$NaGdF_4$:Yb^{3+},Er^{3+} nanocomposites has been conspicuously quenched. This is due to that the Ag nanoparticles with dark-grey colour can absorb the light of the emission from $NaGdF_4$:Yb^{3+},Er^{3+} nanoparticles. In the inset of Fig. 6, the CIE 1931 chromaticity diagram of $NaGdF_4$:Yb^{3+},Er^{3+} (a) and Ag/$NaGdF_4$:Yb^{3+},Er^{3+} (b) were presented under 980 nm laser excitation. The CIE chromaticity coordinates of $NaGdF_4$:Yb^{3+},Er^{3+} nanoparticles and Ag/$NaGdF_4$:Yb^{3+},Er^{3+} nanocomposites are determined as point a (0.226, 0.629) and point b (0.192, 0.619), which are located in green region, and the green emission light can be observed by the naked eye. Hence, the green emission intensity of the hybrid Ag/$NaGdF_4$:Yb^{3+},Er^{3+} multifunctional nanocomposites is still strong enough for actual applications.

Photothermal transduction properties

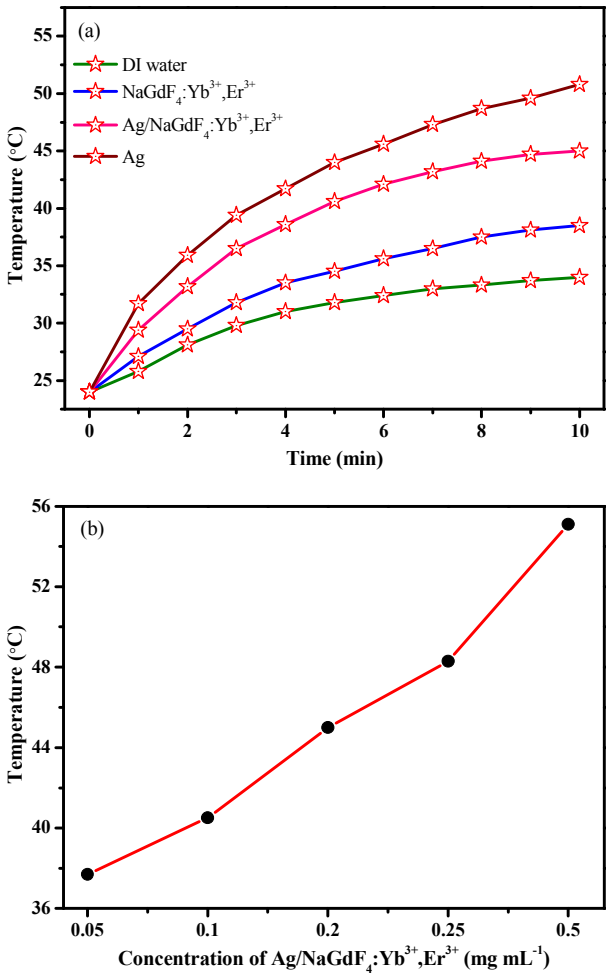

Fig. 7 The temperature of DI water, $NaGdF_4$:Yb^{3+},Er^{3+} nanoparticles, Ag/$NaGdF_4$:Yb^{3+},Er^{3+} nanocomposites and Ag nanoparticles as a function of excitation time (a), the photothermal effect of Ag/$NaGdF_4$:Yb^{3+},Er^{3+} nanocomposites with different concentrations after excitation 10 min with 980 nm laser excitation (b).

To further prove the photothermal transduction efficiency of the

$Ag/NaGdF_4:Yb^{3+},Er^{3+}$ nanocomposites, we exposed the solution of products to a 980 nm NIR laser irradiation at power density of 1.2 W cm^{-2} for 10 min. Because the biomedical materials are always used in *in vivo* or *in vitro* environments, we examined the temperature in aqueous situations of samples. As drawn in Fig. 7a, we observe that the temperatures of DI water, $NaGdF_4:Yb^{3+},Er^{3+}$ and Ag solution are increased from 24.0 °C to 34.0 °C, 38.5 °C and 50.8 °C in 10 min irradiation, respectively, but the temperature of $Ag/NaGdF_4:Yb^{3+},Er^{3+}$ nanocomposites aqueous solution with 0.2 mg mL^{-1} increases to 45.0 °C. In comparison, the temperature changes of DI water, $NaGdF_4:Yb^{3+},Er^{3+}$ and Ag sample confirm that the temperature of the aqueous solution increases mainly from Ag and slightly from DI water and $NaGdF_4:Yb^{3+},Er^{3+}$. We use the same method to investigate the temperature-time curves of the $NaGdF_4:Yb^{3+},Er^{3+}$ nanoparticles, $Ag/NaGdF_4:Yb^{3+},Er^{3+}$ nanocomposites and Ag aqueous solution with different concentrations of (a) 0.05, (b) 0.1, (c) 0.25 and (d) 0.5 mg mL^{-1} , the results were presented in Fig. S1. It can be seen from Fig. S1, the dependence of the samples with different concentrations are same as that of Fig.7a. Fig.7b is the curve of temperature dependence with concentration in hybrid nanocomposites, as shown in Fig. 7b, with increasing the concentration of the nanocomposites, the final temperature of the aqueous solution increases. As the concentration of $Ag/NaGdF_4:Yb^{3+},Er^{3+}$ nanocomposites increases from 0.05 to 0.5 mg mL^{-1}, the obvious temperature increment from 13.7 to 31.1 °C is found. To sum up, we know that the $Ag/NaGdF_4:Yb^{3+},Er^{3+}$ nanocomposites have an outstanding photothermal transduction property and the temperature can be easily controlled by adjusting the concentration of nanocomposites. In addition, the tumor cells can be killed if the temperature increases from 37 °C (body temperature) to 43 °C. In view of the fact that the photothermal effect of the hybrid $Ag/NaGdF_4:Yb^{3+},Er^{3+}$ multifunctional nanocomposites is significant, so we employed them as photothermal agents in cancerous areas and other tissues.

Paramagnetic properties

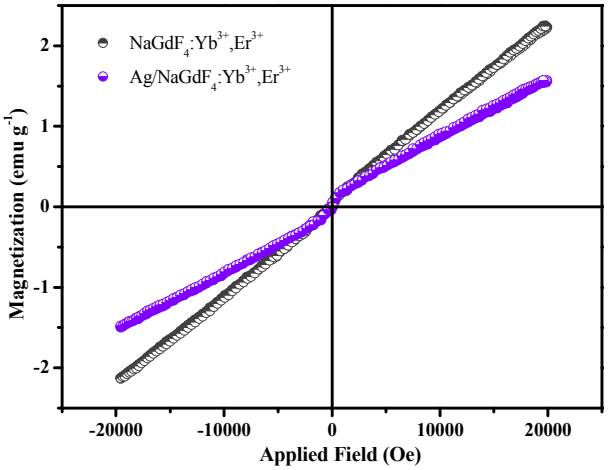

Fig. 8 The magnetization curves of $NaGdF_4:Yb^{3+},Er^{3+}$ nanoparticles and $Ag/NaGdF_4:Yb^{3+},Er^{3+}$ nanocomposites at room temperature.

The magnetic properties of the as-synthesized products were evaluated by VSM at room temperature in the fields between -20 and 20 kOe, the magnetization curves of pure $NaGdF_4:Yb^{3+},Er^{3+}$ nanoparticles and $Ag/NaGdF_4:Yb^{3+},Er^{3+}$ nanocomposites are shown in Fig. 8, respectively. From the magnetic hysteresis loops, we can see that the as-prepared pure $NaGdF_4:Yb^{3+},Er^{3+}$ and $Ag/NaGdF_4:Yb^{3+},Er^{3+}$ both show paramagnetic property due to no coercivity or remanence. The magnetization is found to be about 2.2295 and 1.5669 emu g^{-1} at 20 kOe, respectively, which can be found that the magnetization value reduces approximately 0.66 emu g^{-1} by introducing Ag nanoparticles. The lower measured magnetization value can be attributed to the existence of the diamagnetism contribution of Ag nanoparticles in the $Ag/NaGdF_4:Yb^{3+},Er^{3+}$ nanocomposites, which results in low mass fraction of the pure $NaGdF_4:Yb^{3+},Er^{3+}$ magnetism substance in the multifunctional nanocomposites. Despite the saturation magnetization value is decreased, its strength can be applied in practice. Thus, the hybrid $Ag/NaGdF_4:Yb^{3+},Er^{3+}$ multifunctional nanocomposites could act as an efficient paramagnetic relaxation agent for the magnetic resonance imaging (MRI) and ordinary bioseparation.

Cell viability assays

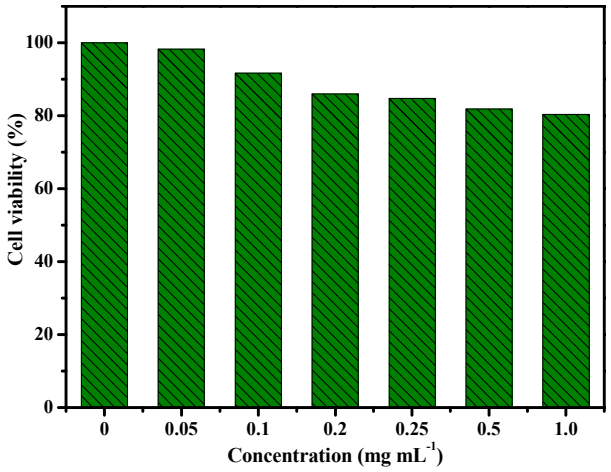

Fig. 9 The cell viability of U87MG cells after incubated with different concentrations of $Ag/NaGdF_4:Yb^{3+},Er^{3+}$ nanocomposites for 24 h.

The excellent luminescence, photothermal and magnetism properties endow the $Ag/NaGdF_4:Yb^{3+},Er^{3+}$ nanocomposites with potential biomedical applications. Hence, evaluating the cytotoxicity of the nanocomposites is especially prerequisite and crucial for biological applications. The cytotoxicity of the nanocomposites towards U87MG cells was investigated by the MTT assay. The standard MTT assay depends on the mitochondrial activity of cells and represents a viable parameter for reporting metabolic activity. Fig. 9 displays the cells viability of U87MG cells after 24 h incubated with a series of concentrations of $Ag/NaGdF_4:Yb^{3+},Er^{3+}$ nanocomposites. It is obviously observed that the nanocomposites exhibit a negligible cytotoxicity profile even at high doses of nanocomposites after incubated for 24 h with $Ag/NaGdF_4:Yb^{3+},Er^{3+}$ nanocomposites at different concentrations of 0.05, 0.1, 0.2, 0.25, 0.5 and 1.0 mg mL^{-1}. It should be noted that the U87MG cells viability is no evident changes when incubated at the concentration of 1.0 mg mL^{-1}. The MTT assay results indicate that the $Ag/NaGdF_4:Yb^{3+},Er^{3+}$ nanocomposites display no cytotoxicity towards the U87MG cells, indicative of good biocompatibility

and potential biomedical application.

Up-conversion luminescence imaging

The MTT-based cell viability assays show that the hybrid Ag/$NaGdF_4$:Yb^{3+},Er^{3+} multifunctional nanocomposites exhibit a negligible cytotoxicity. In order to further verify that the nanocomposites can be used as a cell imaging agent, the up-conversion luminescence images were investigated by inverted up-conversion luminescence microscopy (UCLM). We used time course UCLM to investigate the interaction between the U87MG cells and the Ag/$NaGdF_4$:Yb^{3+},Er^{3+} nanocomposites. For UCL imaging assay, the U87MG cells exhibit evident green luminescence excited by 980 nm laser after incubated with Ag/$NaGdF_4$:Yb^{3+},Er^{3+} nanocomposites (0.25 mg mL^{-1}) at 37 °C for 30 min, 2 h and 4 h. When the cells incubated with nanocomposites at the concentration of 0.25 mg mL^{-1}, the cell viability was detected to be 84.68 % (Fig. 9). As shown in Fig. 10, it illustrates the bright field, cell nucleus, up-conversion luminescent (UCL) imaging and merged images of U87MG cells. At the same time, the gradually enhanced green emission confirms more and more Ag/$NaGdF_4$:Yb^{3+},Er^{3+} nanocomposites were taken up by the cells with the increased incubation time. One can see that in Fig. 10a-d, a weak UCL signal was shown after incubated for 30 min, implying a few of nanocomposites were internalized by U87MG cells. After incubated for 2h (Fig. 10e-h), the green-emitting gradually increased in the cytoplasm. As presented in Fig. 10i-l, the incubation time was prolonged 4 h, the stronger UCL signal could be seen which indicated that a large number of nanocomposites were distributed in the cytoplasmic region of the U87MG cells. This phenomenon suggests that the as-synthesized Ag/$NaGdF_4$:Yb^{3+},Er^{3+} nanocomposites were well accumulated and taken up in the cell cytoplasm, and the signals mainly originated from the cell cytoplasm rather than cell surface, and then the hybrid Ag/$NaGdF_4$:Yb^{3+},Er^{3+} nanocomposites can be used for cell imaging and monitoring the cell endocytosis process.

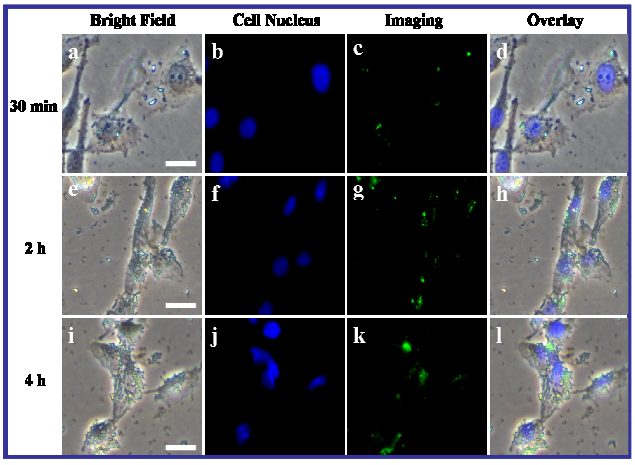

Fig. 10 Inverted luminescence microscope images of U87MG cells incubated with Ag/$NaGdF_4$:Yb^{3+},Er^{3+} nanocomposites for 30 min (a-d), 2 h (e-h) and 4 h (i-l) at 37 °C. Each series can be classified to the bright field images, cell nucleus images (being dyed in blue by DAPI for visualization) in dark field, up-conversion luminescent images (UCL) in dark field and the overlay of the three above, respectively. All scale bars are 100 μm.

Effect of photothermal therapy

As mentioned earlier the Ag nanoparticles are effective photothermal transduction agent, which can be used as molecular antennas to absorb the NIR region and convert the NIR to heat through the SPR, so they have been widely used in photothermal therapy of cancer cells. Further experiments were taken to evaluate the cancer cells inhibition efficacy of the Ag/$NaGdF_4$:Yb^{3+},Er^{3+} nanocomposites under 980 nm laser irradiation *in vitro*. As shown in Fig. 11, the U87MG cells (incubated for 20 h) were exposed to a 980 nm NIR laser irradiation at power density of 1.2 W cm^{-2} for different times in the control group and in the presence of $NaGdF_4$:Yb^{3+},Er^{3+} nanoparticles (a dosage of 0.25 mg mL^{-1}) and Ag/$NaGdF_4$:Yb^{3+},Er^{3+} nanocomposites (a dosage of 0.25 mg mL^{-1}), and the cell viabilities were determined with a MTT assay. Moreover, the treatment with 980 nm NIR laser irradiation resulted in a time-dependent inhibition efficacy of the cell viability. When the irradiation time was 0, 1, 2, 4 and 8 min, the viability of the control group, the group treated with nanoparticles and hybrid nanocomposites of the U87MG cells were detected to be 100, 99.77, 95.37, 92.79, 90.60 %, 97.61, 93.65, 87.70, 82.89, 76.59 % and 92.33, 77.22, 61.15, 29.86, 15.29 %, respectively. We can see that the group treated with hybrid nanocomposites proved the best tumor growth inhibition efficacy. In addition, the longer the irradiation time, the less the cell viability. The results reveal that the hybrid Ag/$NaGdF_4$:Yb^{3+},Er^{3+} nanocomposites have preferable photothermal therapy effects.

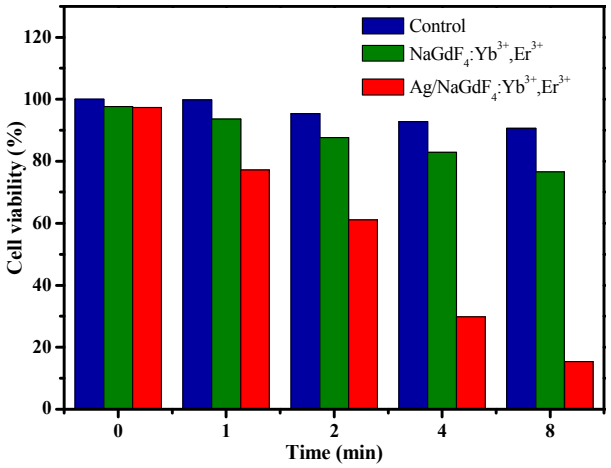

Fig. 11 The cell viability after being irradiated for different times with a 980 nm NIR laser at power density of 1.2 W cm^{-2}.

4. Conclusions

In summary, the hybrid multifunctional nanocomposites have been synthesized combining the $NaGdF_4$:Yb^{3+},Er^{3+} and Ag nanoparticles through a facile solution method. The hybrid nanocomposites exhibit bright up-conversion luminescence under irradiation with a 980 nm laser and magnetism property with room-temperature magnetization value of 1.5669 emu g^{-1} at 20 kOe. Upon 980 nm laser excitation, the solution temperature of Ag/$NaGdF_4$:Yb^{3+},Er^{3+} nanocomposites is obviously raised up in 10 min, owing to the photothermal transduction property of Ag nanoparticles. Simultaneously, the temperature can be changed by adjusting the concentration of nanocomposites. *In vitro*

cytotoxicity assays on U87MG cells demonstrated that the nanocomposites exhibited the low toxicity and good biocompatibility. Furthermore, the Ag/$NaGdF_4$:Yb^{3+},Er^{3+} nanocomposites were allowed to take up by the U87MG cells, the up-conversion luminescence imaging exhibited green emission and the photothermal therapy found to undergo photothermally induced death under 980 nm NIR laser, confirming the nanocomposites potential candidates as bioimaging and photothermal agents. Taken together, these results indicate that the hybrid Ag/$NaGdF_4$:Yb^{3+},Er^{3+} multifunctional nanocomposites based luminescence-photothermal-magnetism properties have great promise in the future bioimaging and targeted therapy of tumor.

Acknowledgements

This work was supported by the National Natural Science Foundation of P.R. China (NSFC) (Grant No. 51072026, 51573023) and the Development of science and technology plan projects of Jilin province (Grant No. 20130206002 GX)

Notes and references

Key Laboratory of Applied Chemistry and Nanotechnology at Universities of Jilin Province, Changchun University of Science and Technology, Changchun 130022, P. R. China. E-mail address: liuguixia22@163.com; Tel.:+86-431-85582574. Fax: +86-431-85383815.

1 X. Michalet, F. F. Pinaud, L. A. Bentolila, J. M. Tsay, S. Doose, J. J. Li, G. Sundaresan, A. M. Wu, S. S. Gambhir and S. Weiss, *Science,* 2005, **307**, 538-544.
2 Y. Piao, A. Burns, J. Kim, U. Wiesner and T. Hyeon, *Adv. Funct. Mater.,* 2008, **18**, 3745-3758.
3 X. Kang, Z. Cheng, D. Yang, P. A. Ma, M. Shang, C. Peng, Y. Dai and J. Lin, *Adv. Funct. Mater.,* 2012, **22**, 1470-1481.
4 F. Zhang, G. B. Braun, A. Pallaoro, Y. Zhang, Y. Shi, D. Cui, M. Moskovits, D. Zhao and G. D. Stucky, *Nano Lett.,* 2012, **12**, 61-67.
5 H. Xing, W. Bu, S. Zhang, X. Zheng, M. Li, F. Chen, Q. He, L. Zhou, W. Peng, Y. Hua and J. Shi, *Biomaterials,* 2012, **33**, 1079-1089.
6 H. Xing, W. Bu, Q. Ren, X. Zheng, M. Li, S. Zhang, H. Qu, Z. Wang, Y. Hua, K. Zhao, L. Zhou, W. Peng and J. Shi, *Biomaterials,* 2012, **33**, 5384-5393.
7 M. Ma, H. Chen, Y. Chen, X. Wang, F. Chen, X. Cui and J. Shi, *Biomaterials,* 2012, **33**, 989-998.
8 F. Wang, X. Chen, Z. Zhao, S. Tang, X. Huang, C. Lin, C. Cai and N. Zheng, *J. Mater. Chem.,* 2011, **21**, 11244-11252.
9 Y. Chen, Q. Yin, X. Ji, S. Zhang, H. Chen, Y. Zheng, Y. Sun, H. Qu, Z. Wang, Y. Li, X. Wang, K. Zhang, L. Zhang and J. Shi, *Biomaterials,* 2012, **33**, 7126-7137.
10 Y. Chen, H. Chen, S. Zhang, F. Chen, S. Sun, Q. He, M. Ma, X. Wang, H. Wu, L. Zhang, L. Zhang and J. Shi, *Biomaterials,* 2012, **33**, 2388-2398.
11 M. Liong, J. Lu, M. Kovochich, T. Xia, S. G. Ruehm, A. E. Nel, F. Tamanoi and J. I. Zink, *ACS Nano,* 2008, **2**, 889-896.
12 H. Zou, S. Wu and J. Shen, *Chem. Rev.,* 2008, **108**, 3893-3957.
13 F. Wang, D. Banerjee, Y. Liu, X. Chen and X. Liu, *Analyst,* 2010, **135**, 1839-1854.
14 Q. Ju, D. Tu, Y. Liu, R. Li, H. Zhu, J. Chen, Z. Chen, M. Huang and X. Chen, *J. Am. Chem. Soc.,* 2012, **134**, 1323-1330.
15 G. Yang, S. Gai, F. Qu and P. Yang, *ACS Appl. Mat. Interfaces,* 2013, **5**, 5788-5796.
16 L. Zhang, Y. S. Wang, Y. Yang, F. Zhang, W. F. Dong, S. Y. Zhou, W. H. Pei, H. D. Chen and H. B. Sun, *Chem. Commun.,* 2012, **48**, 11238-11240.
17 W. Liu, G. Liu, X. Dong, J. Wang and W. Yu, *Phys. Chem. Chem. Phys.,* 2015, **17**, 22659-22667.
18 H. Arimoto and M. Egawa, *Skin Research and Technology,* 2015, **21**, 94-100.
19 F. Chen, W. Bu, S. Zhang, J. Liu, W. Fan, L. Zhou, W. Peng and J. Shi, *Adv. Funct. Mater.,* 2013, **23**, 298-307.
20 X. Liu, R. Deng, Y. Zhang, Y. Wang, H. Chang, L. Huang and X. Liu, *Chem. Soc. Rev.,* 2015, **44**, 1479-1508.
21 S. Wang, J. Feng, S. Song and H. Zhang, *CrystEngComm,* 2013, **15**, 7142-7151.
22 H. Liu, W. Lu, H. Wang, L. Rao, Z. Yi, S. Zeng and J. Hao, *Nanoscale,* 2013, **5**, 6023-6029.
23 B. Chen, B. Dong, J. Wang, S. Zhang, L. Xu, W. Yu and H. Song, *Nanoscale,* 2013, **5**, 8541-8549.
24 V. A. Lebedev, V. F. Pisarenko, N. V. Selina, A. A. Perfilin and M. G. Brik, *Opt. Mater.,* 2000, **14**, 121-126.
25 W. Xu, S. Xu, Y. Zhu, T. Liu, X. Bai, B. Dong, L. Xu and H. Song, *Nanoscale,* 2012, **4**, 6971-6973.
26 A. Noculak, A. Podhorodecki, G. Pawlik, M. Banski and J. Misiewicz, *Nanoscale,* 2015, **7**, 13784-13792.
27 B. Zhou, Y. Wang and D. Xia, *RSC Adv.,* 2015, **5**, 66807-66814.
28 J. Zhang, Z. Hao, J. Li, X. Zhang, Y. Luo and G. Pan, *Light Sci Appl,* 2015, **4**, e239.
29 R. Wang and F. Zhang, *J. Mater. Chem. B,* 2014, **2**, 2422-2443.
30 S. S. Lucky, N. Muhammad Idris, Z. Li, K. Huang, K. C. Soo and Y. Zhang, *ACS Nano,* 2015, **9**, 191-205.
31 S. Cui, D. Yin, Y. Chen, Y. Di, H. Chen, Y. Ma, S. Achilefu and Y. Gu, *ACS Nano,* 2013, **7**, 676-688.
32 G. Yang, R. Lv, F. He, F. Qu, S. Gai, S. Du, Z. Wei and P. Yang, *Nanoscale,* 2015, **7**, 13747-13758.
33 L. Zeng, L. Luo, Y. Pan, S. Luo, G. Lu and A. Wu, *Nanoscale,* 2015, **7**, 8946-8954.
34 Y. Hu, L. Meng, L. Niu and Q. Lu, *ACS Appl. Mater. Interfaces,* 2013, **5**, 4586-4591.
35 G. Xiang, J. Zhang, Z. Hao, X. Zhang, G.-H. Pan, Y. Luo and H. Zhao, *CrystEngComm,* 2015, **17**, 3103-3109.
36 S. Zeng, M.-K. Tsang, C.-F. Chan, K.-L. Wong and J. Hao, *Biomaterials,* 2012, **33**, 9232-9238.
37 J. Wang, F. Wang, C. Wang, Z. Liu and X. Liu, *Angew. Chem. Int. Ed.,* 2011, **50**, 10369-10372.
38 Q. Liu, Y. Sun, T. Yang, W. Feng, C. Li and F. Li, *J. Am. Chem. Soc.,* 2011, **133**, 17122-17125.
39 L. Cheng, K. Yang, Y. Li, J. Chen, C. Wang, M. Shao, S.-T. Lee and Z. Liu, *Angew. Chem. Int. Ed.,* 2011, **50**, 7385-7390.
40 X. Chen, Z. Zhao, M. Jiang, D. Que, S. Shi and N. Zheng, *New J. Chem.,* 2013, **37**, 1782-1788.
41 Y. Sun, B. Wiley, Z.-Y. Li and Y. Xia, *J. Am. Chem. Soc.,* 2004, **126**, 9399-9406.
42 J. Lin, S. Wang, P. Huang, Z. Wang, S. Chen, G. Niu, W. Li, J. He, D. Cui, G. Lu, X. Chen and Z. Nie, *ACS Nano,* 2013, **7**, 5320-5329.
43 B. Dong, S. Xu, J. Sun, S. Bi, D. Li, X. Bai, Y. Wang, L. Wang and H. Song, *J. Mater. Chem.,* 2011, **21**, 6193-6200.
44 L. Dykman and N. Khlebtsov, *Chem. Soc. Rev.,* 2012, **41**, 2256-2282.
45 Y. Song, G. Liu, X. Dong, J. Wang, W. Yu and J. Li, *J. Phys. Chem. C,* 2015, **119**, 18527-18536.
46 H. Zheng, B. Zou, L. Chen, Y. Wang, X. Zhang and S. Zhou, *CrystEngComm,* 2015, **17**, 6393-6398.
47 Y. Song, G. Liu, J. Wang, X. Dong and W. Yu, *Phys. Chem. Chem. Phys.,* 2014, **16**, 15139-15145.
48 Y. Song, G. Liu, X. Dong, J. Wang, W. Yu and J. Li, *RSC Adv.,* 2014, **4**, 62802-62808.
49 C.-W. Chen, P.-H. Lee, Y.-C. Chan, M. Hsiao, C.-H. Chen, P. C. Wu, P. R. Wu, D. P. Tsai, D. Tu, X. Chen and R.-S. Liu, *J. Mater. Chem. B,* 2015.
50 J. Lee and D.-J. Jang, *RSC Adv.,* 2015, **5**, 64268-64273.
51 Y. Liu and Y. Sun, *Nanoscale,* 2015, **7**, 13687-13693.
52 X. Huang, I. H. El-Sayed, W. Qian and M. A. El-Sayed, *J. Am. Chem. Soc.,* 2006, **128**, 2115-2120.
53 A. M. Gobin, M. H. Lee, N. J. Halas, W. D. James, R. A. Drezek and J. L. West, *Nano Lett.,* 2007, **7**, 1929-1934.
54 D. Boyer, P. Tamarat, A. Maali, B. Lounis and M. Orrit, *Science,* 2002, **297**, 1160-1163.
55 P. Khoza, E. Antunes, J.-Y. Chen and T. Nyokong, *J. Lumin.*, 2013, **134**, 784-790.

Graphical Abstract

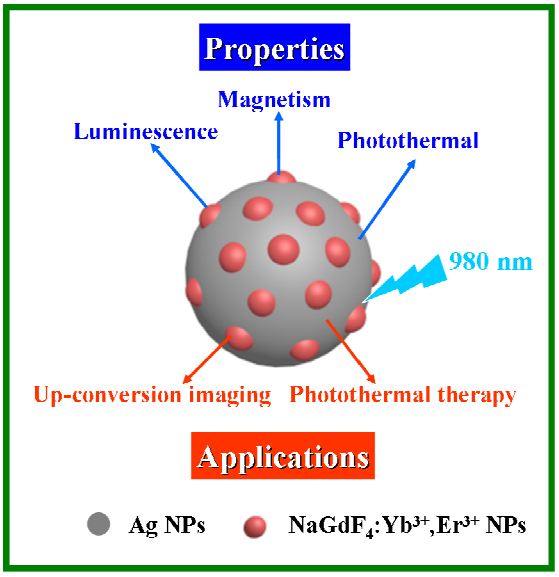

The novel hybrid Ag/$NaGdF_4$:Yb^{3+},Er^{3+} multifunctional nanocomposites based on luminescence-photothermal-magnetism properties have great promise in the future up-conversion luminescence imaging and photothermal therapy of tumor.